Tetrahedron 64 (2008) 8738–8745

Contents lists available at ScienceDirect

Tetrahedron

journal homepage: www.elsevier.com/locate/tet

Synthesis of bifluorene-based molecular materials: effect of C-9 spirocyclohexane functionalization and end-group tailoring

Roberto Grisorio [a], Claudia Piliego [b,c], Pinalysa Cosma [e], Paola Fini [f], Piero Mastrorilli [a], Giuseppe Gigli [b,d], Gian Paolo Suranna [a,*], Cosimo Francesco Nobile [a]

[a] Dipartimento di Ingegneria delle Acque e di Chimica (DIAC), Politecnico di Bari, via Orabona 4, I-70125 Bari, Italy
[b] National Nanotechnology Laboratories (NNL) of CNR-INFM, Lecce, Italy
[c] Istituto Superiore Universitario di Formazione Interdisciplinare (ISUFI)-sezione Nanoscienze, Lecce, Italy
[d] Dipartimento di Ingegneria dell'Innovazione, Università del Salento, Lecce, Italy
[e] Dipartimento di Chimica dell'Università di Bari, Campus Universitario, Bari, Italy
[f] IPCF-CNR, c/o Dipartimento di Chimica, Bari, Italy

ARTICLE INFO

Article history:
Received 8 April 2008
Received in revised form 10 June 2008
Accepted 26 June 2008
Available online 28 June 2008

Keywords:
Spiro compounds
Alkynes
Fluorene
Carbazole
OLED

ABSTRACT

The preparation and properties of the first spirocyclohexane-functionalized bifluorene-based monodispersed molecular materials is described. The obtained compounds were characterized by ^{1}H NMR, ^{13}C{^{1}H} NMR, IR, DSC, UV–vis and photoluminescence both in solution and in the solid state. The molecules show emissions ranging from the blue to the blue-green region, and higher glass transition temperatures and spectral stability with respect to the analogous compounds containing 9,9,9′,9′-tetrahexyl-[2,2′]-bifluorene core. The materials were used as active layers in electroluminescent devices with ITO/PEDOT-PSS/**SB1**–**4**/Ca/Al and ITO/PEDOT-PSS/**SB1**–**4**/BCP/Ca/Al configurations.

1. Introduction

Research on organic optical materials received a boost by the development of π-conjugated structures containing as motif two adjacent phenylene rings covalently bound by a methylene link.[1] The interest for fluorene systems has been sustained mainly by their versatility, deriving from the acidity of the methylene hydrogen atoms that can consequently be easily functionalized with a variety of substituents. This chemistry led to the preparation of a huge number of fluorene-based structures bearing alkyl groups at the C-9 position that were used essentially as building blocks for the synthesis of blue-emitting polyfluorenes for OLED applications.[2] However, the valuable blue emission of most polyfluorenes is stained by the appearance of a low-energy emission band falling in the green region. The debate on the origin of this green emission, characterized by two opposite points of view, associating the spectral instability of polyfluorenes either to on-chain defect emission[3] or to fluorenone-based excimer formation,[4] has now ascertained that the appearance of the green band is correlated with degradation processes involving the fluorene C-9 position.[5] Well-defined oligomeric structures can indeed lower the complexity connected with the study of polymeric materials; due to their greater ease of purification and characterization, more precise structure–property relations can be drawn and the effects of substituents on the behaviour of a defined chemical structure can be better assessed.[6] Moreover, monodispersed oligofluorenes have shown the suitable prerequisites for their use as active layers in blue OLED, due to their higher stability with respect to the corresponding polymers.[7] The introduction of suitable end groups onto the oligofluorene backbone can exert a deep influence on the optical properties, the ionization potential and the electron affinity of the corresponding structures, an aspect that makes monodispersed organic materials more versatile with respect to the corresponding polymers. For instance, an important goal that can be achieved by the judicious placing of electron donating and/or electron withdrawing groups onto the fluorene core is the improvement of the balancing between hole and electron transport within the OLED active film, a factor that may eventually lead to a simplification of the device configurations.[8] Concerning the C-9 functionalization of the fluorene backbone, spiro substitution aimed at the formation of spirobifluorene building blocks has been studied in depth.[9] A simpler fluorene C-9 functionalization can be obtained by

* Corresponding author. Tel.: +39 080 5963603; fax: +39 080 5963611.
E-mail address: surannag@poliba.it (G.P. Suranna).

0040-4020/$ – see front matter © 2008 Elsevier Ltd. All rights reserved.
doi:10.1016/j.tet.2008.06.098

endowing the fluorene with a sufficiently large spirocycloalkane. The advantages of such substitution reside in the reduction of coplanar interactions between adjacent molecules in the solid state as well as in the potentially higher glass transition temperatures of the materials, properties that have a positive influence on OLED performance. In this perspective, we have recently described the synthesis of new spirocyclohexane-functionalized polyfluorenes and found that the incorporation of a stiff spirocyclohexane moiety did endow the polymers with higher glass transition temperatures and higher spectral stability with respect to poly(dialkylfluorene)s.[10]

By linking two fluorene units through the 2,2′-position, the simplest fluorene oligomer, i.e., bifluorene, is obtained. However, the 7,7′-functionalization of a bifluorene core, aimed at tailoring its properties, has been explored only to a limited extent.[8a,11] The intriguing properties of the bifluorene core and the potentialities of the spirocycloalkane substitution, so far unexplored for oligomers, motivated our choice to embark in the synthesis and study of the properties of monodispersed molecular materials obtained by linking (a) 9,9-dihexyl-fluoren-2-yl, (b) *N*-hexyl-carbazol-3-yl and (c) 5-carbodecaoxy-2,2′-bithien-5′-yl groups to a spirocyclohexane C-9-functionalized bifluorene building block. These functional groups were linked to the 7,7′ positions of the bifluorene core through triple bonds, a conjugation extension approach followed until now only for a few fluorene systems.[12]

The results obtained with these symmetrical bifluorene oligomers were compared with those of an unsymmetrically functionalized bifluorene-based molecular material containing both the electron withdrawing (5-carbodecaoxy-2,2′-bithien-5′-yl-ethynyl) and the electron donating (*N*-hexyl-carbazol-3-yl-ethynyl) groups.

2. Results and discussion

2.1. Synthesis and thermal properties

The retrosynthetic approach followed for the synthesis of the target molecules **SB1**–**4** envisaged a disconnection at the 7,7′ positions of the spirocyclohexane-bifluorene core. As outlined in Scheme 1, the first task was the synthesis of the reactive bifluorene core **4**. In order to avoid the potentially unselective direct halogenation of a bifluorene structure, we approached the synthesis of **4** by applying the $Ni(cod)_2$-promoted homocoupling of 2-bromo-7-trimethylsilyl fluorene.[13] For our purposes, the preparation started from 2,7-dibromofluorene, the reaction of which with 1,5-dibromopentane afforded the spiro-derivative **1** in 66% yield. The reaction was carried out in toluene/NaOH (aq) (1:1 v/v). Biphasic reaction conditions were previously found to be the best ones in order to maximize the yield of the ring closure.[10b] The next step was the mono-functionalization of **1** to create the intermediate for dimerization. The interconversion of one of the bromides into a trimethylsilyl group as 'dormant iodide' was achieved by reaction of **1** with 1 equiv of *n*-BuLi and subsequent reaction with trimethylsilyl chloride. The spiro-derivative **2** was obtained in 97% yield. At this stage, the homocoupling of **2** promoted by $Ni(cod)_2$ afforded the bis-functionalized bifluorene building block **3** in 76% yield. The synthesis of **4** was accomplished in 88% yield by iododesilylation with ICl. With respect to the analogous tetraalkyl bifluorenes, the building block **4** was considerably less soluble in halogenated solvents such as methylene chloride and chloroform.

Following our convergent-divergent approach, we tagged the synthesis of the fluorene, carbazole and bithienyl alkynes (Scheme 2). The building blocks 2-ethynyl-9,9-dihexyl-fluorene (**5**) and 3-ethynyl-*N*-hexyl-carbazole (**6**) were prepared following a previously published synthetic approach.[14] The intermediate **8** was obtained in 85% yield by reaction of the acyl-chloride **7** with decan-1-ol in presence of pyridine. A Sonogashira coupling of **8** with trimethylsilylacetylene, catalyzed by $PdCl_2(PPh_3)_2$/CuI afforded the corresponding intermediate **9** in 80% yield, which was deprotected by reaction with potassium fluoride to give the terminal alkyne **10** in 95% yield. Due to decomposition problems, compound **10** had to be promptly used in the following reaction step.

Eventually, we carried out the synthesis of the target bifluorenes **SB1**–**4** (Scheme 2). For **SB1** and **SB2**, a straightforward Sonogashira coupling between **4** and 2 equiv of the suitable alkynes **5** and **6**, respectively, was performed. The reaction was carried out with a different catalytic system, namely $Pd(PPh_3)_4$/CuI in order to minimize the amount of byproducts deriving from the homocoupling of the alkynes, and allowed the obtainment of both target molecules in 81% yield. We decided to carry out the preparation of the **SB3** target by reacting **4** with an equimolar amount of the alkyne **10**. Under these conditions, **SB3** was obtained in 17% yield, but the reaction simultaneously gave the iodo-derivative **11**, which could be isolated in 27% yield and subsequently be employed for the synthesis of the unsymmetrically substituted **SB4**. The latter was obtained in 93% yield by a Pd-catalyzed cross coupling with an equimolar amount of **6**. ^1H NMR, $^{13}C\{^1H\}$ NMR, IR and elemental analysis confirmed the identity and the purity of **4** and of **SB1**–**4** (see Supplementary data).

An interesting NMR feature of this class of compounds is the chemical shift of the β-methylene groups in the spirocyclohexane substitution. In the ^1H NMR spectrum of 9,9-di-(*n*-alkyl)fluorene derivatives, the methylene protons in the β-position are shielded to ~0.6 ppm and resonate at higher fields even with respect to the methyl protons. On the other hand, in fluorene spirocyclohexane derivatives (for instance, in the bifluorene intermediate **3**), the methylene protons signals are constituted by two groups of signals: a multiplet at 2.09–1.96 ppm (8 protons) and a multiplet at 1.93–1.83 ppm (12 protons). All other bifluorene spirocyclohexane-containing molecules show an analogous pattern. Aiming at discriminating the chemical shift of the three groups of methylene protons (α, β and γ) in the spirocyclohexane substitution, we investigated the NMR behaviour of the monofluorene spirocyclohexane derivative **1** for which the signal of the three methylene hydrogens fall between 1.90 and 1.80 ppm. Interestingly, the more deshielded protons of these signals were attributed to the β-hydrogen atoms, as indicated by a ^1H–^1H COSY experiment (see

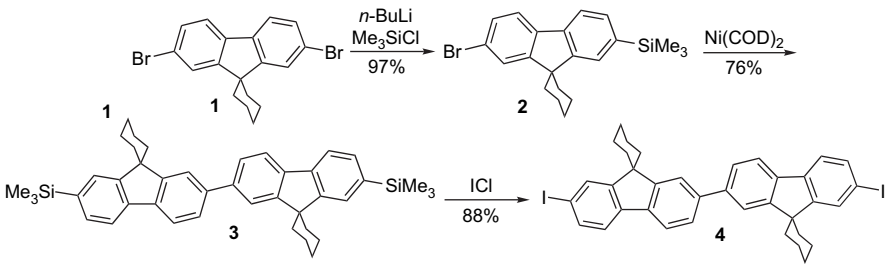

Scheme 1. Synthetic sequence for the synthesis of **4**.

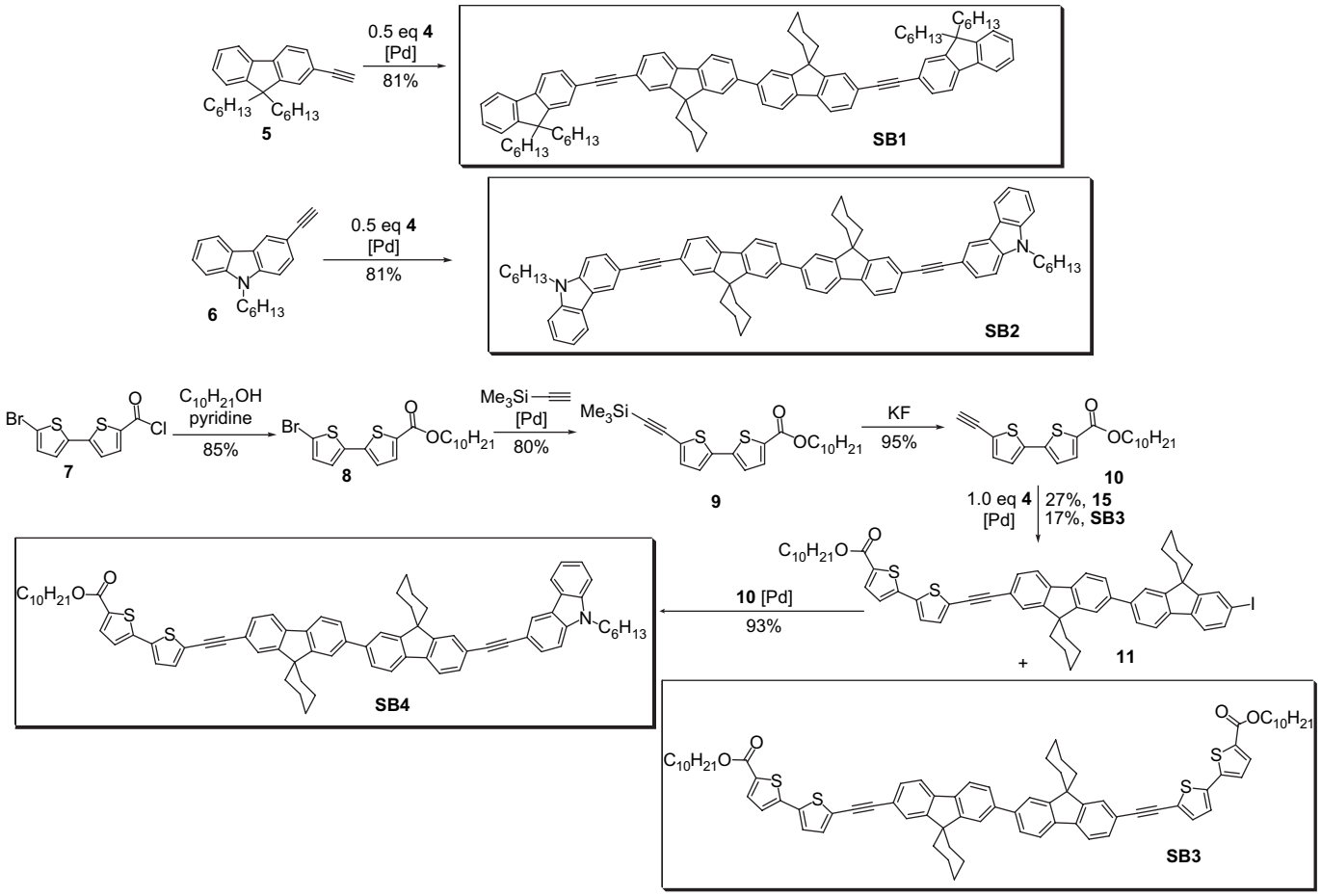

Scheme 2. Synthetic sequence for the obtainment of **SB1–4**.

Supplementary data). Moreover, as indicated by a $^{1}H–^{13}C$ HMQC experiment (see Supplementary data) the corresponding α-methylene carbon resonates at higher field with respect to the other.

Differential scanning calorimetry (DSC) gave insights into the thermal properties of **SB1–4**. The relevant results are collected in Table 1. All materials showed endothermic events during heating scans, which could be attributed to the melting of crystalline portions of the sample, and were not observed during cooling scans. In the second heating scans, events attributable to glass transitions could be observed at 84.7 and 98.5 °C only in the case of **SB1** and **SB2**, respectively. These values are considerably higher (30 and 49 °C) than those exhibited by the corresponding molecules containing the 9,9,9′,9′-tetrahexyl-[2,2′]-bifluorene core[14] due to the stiffness of the spirocyclohexane functionality. Moreover, in the case of **SB3** and **SB4**, no thermal events could be detected, indicating the formation of amorphous phases with negligible glass transitions. The DSC scans did not evidence signs of any decomposition below 250 °C.

2.2. Optical properties

The optical properties of **SB1–4** were studied both in $CHCl_3$ solution and in the solid state. In solution (Fig. 1A and B), the absorption maxima of **SB1** and **SB2** are similar (380 and 378 nm, respectively), the latter showing the expected absorption band at 286 nm caused by the π–π* transition of the carbazole unit excluded from conjugation because of its substitution in the 3-position. The photoluminescence (PL) spectrum of **SB1** showed

Table 1
DSC data and electrochemical properties of **SB1–4**. Features of OLED devices based on **SB1–4** of structure ITO/PEDOT-PSS/**SB1–4**/Ca/Al (type I) and of structure ITO/PEDOT-PSS/**SB1–4**/BCP(7.5 nm)Ca/Al (type II)

	First heating scan (°C)	Second heating scan (°C)	E_{ox}[a] (V)	HOMO[b] (eV)	LUMO (eV)	Energy gap[c] (eV)	Max luminance (cd/m^2)	Max current efficiency (cd/A)	External efficiency[e] (%)	CIE colour coord.[e] (x, y)
SB1	229.5	84.7[d] (T_g)	0.944	−5.53	−2.49	3.04	428 (I)	0.019 (I)	0.010 (I)	0.17, 0.20 (I)
							538 (II)	0.033 (II)	0.020 (II)	0.17, 0.21 (II)
SB2	210.0/234.3	98.5[d] (T_g)	0.657	−5.28	−2.23	3.05	732 (I)	0.011 (I)	0.006 (I)	0.18, 0.17 (I)
							938 (II)	0.073 (II)	0.042 (II)	0.21, 0.22 (II)
SB3	91.3/170.6	—	0.838	−5.44	−2.66	2.78	—	—	—	—
SB4	154.3	—	0.601	−5.27	−2.49	2.78	482 (I)	0.020 (I)	0.012 (I)	0.18, 0.32 (I)
							1005 (II)	0.056 (II)	0.023 (II)	0.19, 0.37 (II)

[a] Onset of oxidation potentials.
[b] Estimated after calibration of the voltammograms by Fc/Fc^{+} internal reference.
[c] Estimated from the onset of absorption in the UV–vis spectrum.
[d] Midpoint of the thermal event.
[e] Data obtained from spectra at 12 V.

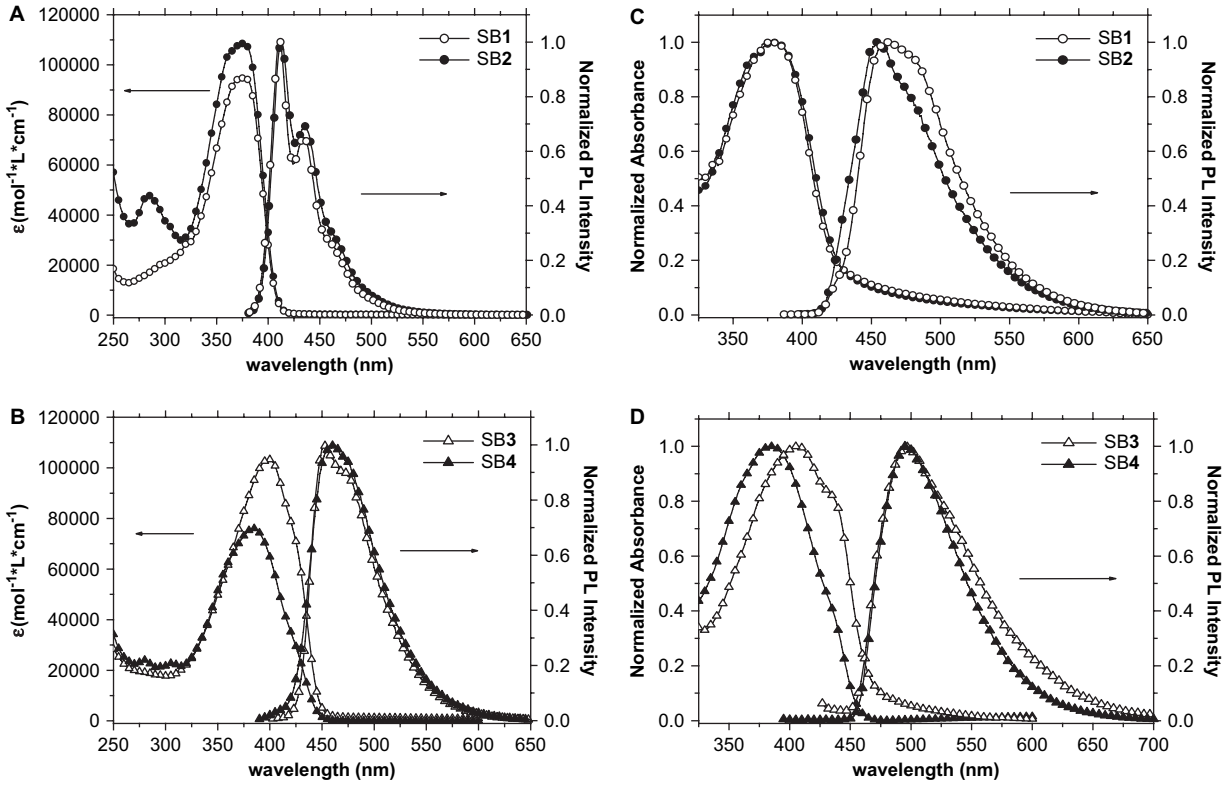

Figure 1. Absorption and PL spectra of **SB1** and **SB2** (A,C), and **SB3** and **SB4** (B,D) in $CHCl_3$ and in the solid state.

a maximum at 413 nm followed by a vibronic replica at 437 nm and is very similar to **SB2** with peaks at 414 and 438 nm. The quantum yields are 0.96 and 0.91, respectively.

Next, we studied the optical properties of the molecules containing the electron withdrawing thiophene-based end group (**SB3** and **SB4**) that was incorporated in the molecular structure as a versatile alternative to the well-known *S*,*S*-dioxide thiophene moiety.[15] The absorption and emission spectra of **SB3** and **SB4** are reported in Figure 1B. In the case of **SB3**, the introduction of two ester functionalized bithiophenes in the structure determines a substantial bathochromic shift of the absorption maximum (λ_{abs}=401 nm), while the asymmetric molecule **SB4**, containing both the carbazole and the bithienyl as end groups, absorbs at 387 nm. Their emission spectra are structureless and show maxima at 454 nm (**SB3**) and 458 nm (**SB4**). The presence of thiophene systems lowered the quantum yield of the compounds (0.39 for **SB3** and 0.47 for **SB4**). Furthermore, the presence of the functionalized bithienyl group in **SB3** and **SB4** causes a remarkable lowering of the energy gap of 0.26 eV with respect to **SB1** and **SB2**, as evaluated by the onset of UV–vis absorption spectra in solution. In order to evaluate the optical behaviour of **SB1**–**4** in the solid state, a spin-coated film of the relevant material on quartz was studied (Fig. 1C and D). The absorption spectra of **SB1** and **SB2** are perfectly superimposable and show a maximum at 379 nm, a λ_{max} similar to those observed in solution. The PL spectra show the loss of the vibronic structure with respect to those recorded in solution and show maxima at λ_{em}=461 nm (**SB1**) and λ_{em}=454 nm (**SB2**). The analysis of the solid state absorption of **SB3** and **SB4** reveals a maximum at 407 nm with a shoulder at 431 nm for **SB3** and a maximum at 383 nm for **SB4**. The PL spectra of **SB3** and **SB4** show the same profile, and both show a λ_{em}=497 nm.

In order to test the spectral stability of the spirocyclohexane-containing materials, we studied the optical behaviour of **SB2** after a UV irradiation of 15 min in air. The results were compared with those obtained by carrying out the same treatment to a film of its analogous embodying a 9,9,9′,9′-tetrahexyl-[2,2′]-bifluorene core (**BF2**).[14]

Contrary to what observed in the case of the tetrahexyl functionalised bifluorene analogue, the appearance of a longer wavelength tail emission deriving from the plausible formation of fluorenones is absent in the case of **SB2** (Fig. 2). This aspect constitutes a clear confirmation of the higher spectral stability of spirocyclohexane-containing fluorene-based materials with respect to 9,9-dialkylfluorene-based ones.

2.3. HOMO–LUMO energy levels

In order to evaluate the influence of the functional groups on the HOMO–LUMO energy levels of **SB1**–**4**, their electrochemical behaviour was studied by cyclic voltammetry (CV). The estimate of the HOMO level was carried out by measuring the onset of oxidation during the first CV scan on thin films of the materials deposited on ITO (indium–tin oxide). As no clear reduction events could be detected during the cathodic scans, the LUMO energy level was calculated by the equation LUMO=HOMO+E_{gap}. The results are collected in Table 1 and in Supplementary data. Changing the end groups from fluorene to carbazole has the effect of lowering the ionization potential (−5.53 eV for **SB1** and −5.28 eV for **SB2**). As a consequence of the similarity of the energy gap, also the LUMO values follow the same trend. The comparison of the HOMO energy levels of **SB3** and **SB4** (−5.44 and −5.27 eV, respectively) confirmed that the introduction of the carbazole moiety in the asymmetric **SB4** compound determines a lowering of the ionization potential with respect to **SB3**.

2.4. Electroluminescence properties

Preliminary electroluminescence (EL) characteristics of **SB1**–**4** were studied by realizing diodes of ITO/PEDOT-PSS/**SB1**–**4**/Ca/Al configuration. Their figures of merit are reported in Table 1. All the tested OLEDs exhibited a turn-on voltage of 4 V, except for the

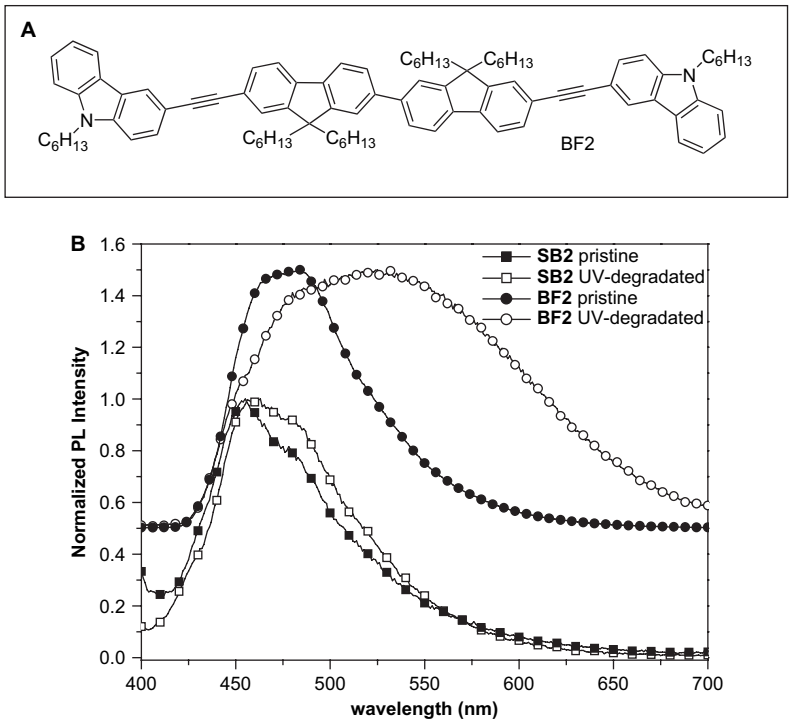

Figure 2. (A) Chemical structure of **BF2** and (B) PL spectra of **BF2** (from Ref. 14) and **SB2** in the solid state after a UV irradiation of 15 min in air.

device embodying **SB3** (6 V). Devices based on **SB1** and **SB2** emit in the sky-blue region, as can be deduced from their CIE coordinates. The OLED embodying **SB1** shows a maximum brightness of 428 cd/m^2 at 12 V with a maximum current efficiency of 0.019 cd/A at 10 V. In the case of **SB2**, current efficiencies are lower (0.011 cd/A at 16 V) than those recorded for **SB1**. However, the devices based on **SB2** can be biased at higher voltages, leading to a higher device performance in terms of maximum luminance (732 cd/m^2 at 18 V). Conversely, the OLED realized with **SB3** as active layer shows an EL spectrum, which is extremely broad and red shifted with respect to the solid state PL (see Supplementary data), and its luminance and current efficiencies are poor. The reasons for these low performances for **SB3** may reside in the formation of excimers or exciplexes, which typically lead to a consistent broadening of the EL spectrum.

It is noteworthy that in the case of **SB4**, which is formally obtained from **SB3** by substitution of one of the two bithienyl groups with an *N*-hexylcarbazolyl moiety, the EL spectrum follows the profile observed in the solid state PL with CIE coordinates falling in the blue-green region. Furthermore, the presence of an electron donating and an electron withdrawing group in the asymmetric structure of **SB4** seems to favour efficient carrier recombination within the active layer, notwithstanding the lower emission ability of the thiophene-containing compound, as the maximum luminance (482 cd/m^2 at 14 V) and the current efficiency (0.020 cd/A at 10 V) are higher than those of **SB1** and **SB2** at low voltages (6–12 V, Fig. 3B). Furthermore, the EL spectra of **SB1**, **SB2** and **SB4** do not show substantial changes with voltage (see Supplementary data).

Since most of the high current density observed in OLED based on **SB1**, **SB2** and **SB4** is due to the mobility of holes, an optimization of the device performances was pursued by inserting 7.5 nm of bathocuproine (BCP) as a hole-blocking layer between the active material and the cathode. A substantial improvement of the current efficiencies of **SB1**, **SB2** and **SB4** was observed after the introduction of the hole blocker, as shown in Figure 3B.

A 7-fold current efficiency increase (0.073 cd/A at 16 V) could be recorded for **SB2**, together with a luminance improvement reaching a maximum of 938 cd/m^2 at 18 V. These features were accompanied by a concomitant remarkable lowering of the current densities with respect to the unoptimized devices based on **SB2** (see Supplementary data). This aspect is likely due to the fact that electrons are more difficultly injected (the turn-on voltage was shifted to 6 V) by the introduction of BCP and that the movement of holes undergoes a higher resistance in the device. In the case of **SB1** and **SB4**, the maximum current efficiency of the optimized devices was improved (0.033 cd/A at 8 V and 0.056 cd/A at 6 V, respectively) and the maximum brightness was increased to 578 cd/m^2 at 14 V (**SB1**) and 1005 cd/m^2 at 12 V (**SB4**). Furthermore, the turn-on voltages of these diodes were found to be almost unaltered (4.5 and 3.5 V for the device embodying **SB1** and **SB4**, respectively). By considering the two sets of electroluminescence data obtained, an explanation of the relatively low performances of **SB2** in the unoptimized diodes can be the strongly predominant hole transport within the active layer, shifting the recombination zone very near to the cathode. The higher current efficiencies of **SB4** with respect to **SB1** and **SB2** at low voltages (4–8 V) obtained in the optimized devices represent a further indication of an improved balanced transport of carriers within the active layer. The results obtained for **SB2** are considerably good for blue-emitting materials containing triple bonds.

3. Conclusions

The synthesis and properties of the first bifluorene-based monodispersed organic materials embodying a spirocyclohexane group at the C-9 positions are described. These compounds were prepared by functionalizing the bifluorene core with two fluoren-2-yl-ethynyl (**SB1**), carbazol-3-yl-ethynyl (**SB2**) and 5-carbodecaoxy-2,2′-bithien-5′-yl-ethynyl (**SB3**) groups, respectively. An unsymmetrical molecular structure was obtained by linking a carbazol-3-yl-ethynyl and a 5-carbodecaoxy-2,2′-bithien-5′-yl-ethynyl (**SB4**) groups onto the bifluorene core. The analysis of the UV–vis absorption in solution revealed that the presence of the functional bithienyl groups in **SB3** and **SB4** has the effect of lowering the energy gap of 0.26 eV with

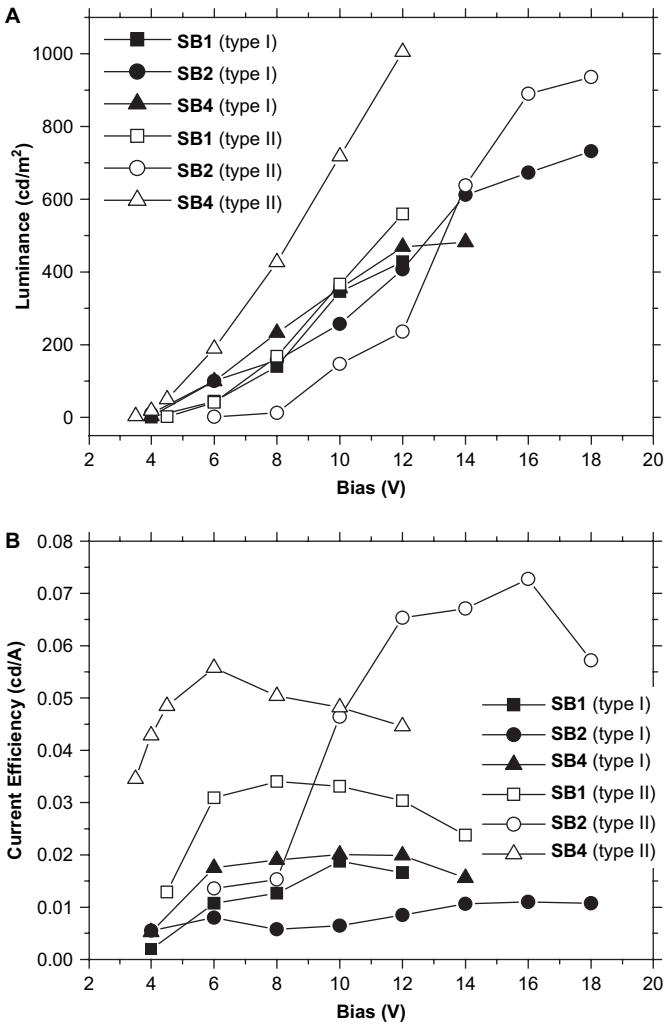

Figure 3. Luminance (A) and current efficiency (B) of OLED of structure ITO/PEDOT-PSS/**SB1**–**4**/Ca/Al (type I) and of structure ITO/PEDOT-PSS/**SB1**–**4**/BCP(7.5 nm)Ca/Al (type II) as a function of bias.

respect to **SB1** and **SB2**. The fluorescence characterization of **SB1** and **SB2** revealed an efficient sky-blue emission in solution and in the solid state. The spiro substitution guarantees a higher glass transition temperature and a higher spectral stability with respect to their tetraalkyl substituted analogues. The EL of the materials was studied by realizing OLEDs with the configuration ITO/PEDOT-PSS/**SB1**–**4**/Ca/Al. The devices showed an emission profile matching the solid state photoluminescence, except for **SB3**, which showed poor EL properties. Noteworthy, it was obtained for the first time a quite respectable EL performance for an organic material (**SB4**) containing a carboxylic ester as functional group. The good performances of **SB1** and **SB4** can be interpreted by a more balanced carrier transport with respect to **SB2**, which shows a behaviour consistent with a predominant hole transport. The introduction of bathocuproine (BCP) as hole-blocking layer permits to improve the performances of **SB1**,and **SB2** and **SB4**. In particular, a 7-fold increase of the current efficiency for **SB2** was recorded due to an efficient recombination of carriers in this optimized device configuration.

4. Experimental section

4.1. General remarks

All manipulations were carried out under an inert nitrogen atmosphere using standard Schlenk techniques. All solvents were carefully dried and freshly distilled prior to use according to common laboratory techniques. NMR spectra were recorded at 295 K on a Bruker Avance 400 MHz spectrometer. UV–vis spectra were recorded on a Kontron Uvikon 942 instrument; fluorescence spectra were obtained on a Varian Cary Eclipse spectrofluorimeter; quantum yields were measured by the dilute solution method, using a 9,10 diphenylanthracene solution in cyclohexane (Φ=0.90) as standard;[16] FTIR spectra were recorded on a Bruker Vector 22 spectrometer. Differential Scanning Calorimetry (DSC) analyses were carried out on a DSC Q200 TA instrument at a scanning rate of 10 °C/min under a nitrogen flow. MS data (EI, 70 eV) were acquired on a HP 6890 instrument equipped with a HP-5MS 5% phenyl methyl siloxane (30.0 m×250 μm×0.25 μm) coupled with a HP 5973 mass spectrometer. UV-photodecomposition experiments were carried out by illuminating the sample with a 150 W high pressure Hg-lamp. Cyclic voltammetry (CV) measurements were carried out under inert nitrogen atmosphere with an Autolab potentiostat PGSTAT 10 using a three-electrode cell. An indium–tin oxide (ITO) electrode was used as the working electrode on which a film of the relevant oligomer was deposited; a Pt wire and a Ag/Ag^+ pseudoreference electrode were utilized as the counter electrode and reference electrode, respectively. All measurements, carried out in acetonitrile solutions of tetrabutylammonium tetrafluoroborate (0.10 M) at a scan rate of 100 mV/s, were calibrated against ferrocene, the ionization potential of which is +4.80 eV.[17] The evaluation of the HOMO level of the materials was carried out by measuring the onset of the oxidation potential in the anodic scan. The OLED devices were prepared by spin coating poly(3,4-ethylenedioxythiophene) poly(styrenesulphonate) (PEDOT-PSS) onto an ITO coated glass substrate previously treated with an O_2-plasma. Subsequently, the active material was spin cast from a chloroform solution (2 mg in 0.3 mL $CHCl_3$) and finally a calcium (45 nm)/aluminum (150 nm) electrode was deposited by thermal evaporation (10^{-6} mbar). For the optimized devices, 2,9-dimethyl-4,7-diphenyl-1,10-phenanthroline (BCP, 7.5 nm) was thermally evaporated before Ca/Al deposition. The characterization of the devices was performed at room temperature in air. The synthesis of **1**[10b] and **7**[18] has been carried out by following the literature procedures.

4.2. 2′-Bromo-7′-trimethylsilyl-spiro(cyclohexane-1,9′-fluorene) (2)

A solution of *n*-BuLi (1.6 M in hexanes, 5.3 mL, 8.45 mmol) was added dropwise to a solution of **1** (3.31 g, 8.45 mmol) in THF (50 mL) kept at −80 °C. The resulting mixture was reacted for 1 h at −80 °C before addition of Me_3SiCl (1.10 g, 10.14 mmol). Then the solution was warmed at room temperature and stirred overnight. After solvent removal, diethyl ether (40 mL) was added and the resulting solution was washed with water (3×20 mL) and dried over Na_2SO_4. After removing the solvent, the crude product was purified by flash chromatography (SiO_2, petroleum ether 40–60 °C) to afford **2** in 97% yield as white solid. Mp=92.3–93.4 °C. MS (EI, 70 eV): *m*/*z* 384.1 (M^+), exact mass: 394.09 uma. Anal. Calcd for $C_{21}H_{25}BrSi$: C, 65.44; H, 6.54. Found: C, 65.42; H, 6.57. ^{1}H NMR (400 MHz, $CDCl_3$): δ=7.94–7.82 (m, 2H), 7.79–7.71 (m, 1H), 7.70–7.49 (m, 3H), 2.10–1.71 (m, 10H), 0.41 (s, 9H) ppm. $^{13}C\{^1H\}$ NMR (100 MHz, $CDCl_3$): δ=155.3, 152.2, 139.6, 139.3, 138.7, 132.2, 130.0, 129.0, 128.0, 121.3, 120.9, 119.3, 50.6, 35.5, 25.6, 22.7, −0.8 ppm.

4.3. 7′,7‴-Bis(trimethylsilyl)-[2′,2‴]-bis[spiro(cyclohexane-1,9′,1″,9‴-fluorene)] (3)

A mixture of **2** (3.00 g, 7.78 mmol), $Ni(cod)_2$ (2.57 g, 9.34 mmol), 2,2′-bipyridine (1.46 g, 9.34 mmol), 1,5-cyclooctadiene (0.84 g, 7.78 mmol) and toluene (50 mL) was stirred overnight at 80 °C.

After cooling to room temperature, the reaction solution was filtered on a Celite® plug, washed with water (3×50 mL) and dried over Na_2SO_4. After removing the solvent, the crude product was purified by flash chromatography (SiO_2, petroleum ether 40–60 °C/CH_2Cl_2=9:1) to afford **3** in 76% yield as white solid. Mp=283.4–284.7 °C. Anal. Calcd for $C_{42}H_{50}Si_2$: C, 82.56; H, 8.25. Found: C, 82.52; H, 8.24. ^{1}H NMR (400 MHz, $CDCl_3$): δ=7.95 (d, J=1.3 Hz, 2H), 7.88–7.83 (m, 4H), 7.80 (d, J=7.6 Hz, 2H), 7.68 (dd, J=7.9, 1.6 Hz, 2H), 7.58 (dd, J=7.6, 1.0 Hz, 2H), 2.09–1.96 (m, 8H), 1.93–1.83 (m, 12H), 0.38 (s, 18H) ppm. ^{13}C{^{1}H} NMR (100 MHz, $CDCl_3$): δ=154.0, 152.7, 140.8, 138.9, 138.7, 132.1, 129.1, 126.3, 123.5, 120.2, 119.2, 50.4, 35.8, 25.7, 22.9, −0.8 ppm.

4.4. 7′,7‴-Diiodo-[2′,2‴]-bis[spiro(cyclohexane-1,9′,1″,9‴-fluorene)] (4)

ICl (1.0 M in CH_2Cl_2, 10.8 mL, 10.84 mmol) was added dropwise at 0 °C to a solution of **3** (1.70 g, 2.78 mmol) in CCl_4 (15 mL). The resulting mixture was stirred at room temperature for 3 h, before portionwise addition of a 10 wt% $Na_2S_2O_3$ aqueous solution until discoloration of the reaction mixture was observed. The organic layer was separated, washed with water (3×30 mL) and dried over Na_2SO_4. After removing the solvent, the crude product was purified by flash chromatography (SiO_2, petroleum ether 40–60 °C/CH_2Cl_2=8:1) to afford **4** in 88% yield as white solid. Mp=297.2–298.4 °C. Anal. Calcd for $C_{36}H_{32}I_2$: C, 60.18; H, 4.49. Found: C, 60.20; H, 4.41. ^{1}H NMR (400 MHz, $CDCl_3$): δ=8.03 (s, 2H), 7.88 (s, 2H), 7.80 (d, J=7.9 Hz, 2H), 7.72 (d, J=7.2 Hz, 2H), 7.64 (d, J=7.2 Hz, 2H), 7.54 (d, J=7.9 Hz, 2H), 2.06–1.90 (m, 8H), 1.89–1.75 (m, 12H) ppm. ^{13}C{^{1}H} NMR (100 MHz, $CDCl_3$): δ=155.6, 153.4, 141.1, 138.9, 137.9, 136.0, 133.7, 126.5, 123.4, 121.6, 120.2, 92.3, 50.6, 35.5, 25.4, 22.6 ppm.

4.5. 5-Bromo-5′-carbodecaoxy-[2,2′]-bithiophene (8)

A mixture of **11** (4.14 g, 13.46 mmol), decan-1-ol (2.13 g, 13.46 mmol), pyridine (1.23 g, 15.50 mmol) and toluene (70 mL) was refluxed overnight. After cooling the solution to room temperature, the mixture was washed with water (3×50 mL) and dried over Na_2SO_4. After removing the solvent, the crude product was purified by flash chromatography (SiO_2, CH_2Cl_2) to afford **8** in 85% yield as pale-yellow solid. Mp=48.8–49.9 °C. Anal. Calcd for $C_{19}H_{25}BrO_2S_2$: C, 53.14; H, 5.87; S, 14.93. Found: C, 53.16; H, 5.89; S, 14.89. ^{1}H NMR (400 MHz, $CDCl_3$): δ=7.67 (d, J=3.9 Hz, 1H), 7.07 (d, J=3.9 Hz, 1H), 7.03–6.99 (m, 2H), 4.28 (t, J=6.7 Hz, 2H), 1.74 (quint, J=6.7 Hz, 2H), 1.45–1.27 (m, 14H), 0.88 (t, J=7.0 Hz, 3H) ppm. ^{13}C{^{1}H} NMR (100 MHz, $CDCl_3$): δ=162.0, 142.7, 137.8, 133.9, 132.3, 130.9, 125.2, 124.0, 112.9, 65.5, 31.9, 29.6, 29.5, 29.3, 28.7, 26.0, 22.7, 14.1 ppm.

4.6. 5-Trimethylsilylethynyl-5′-carbodecaoxy-[2,2′]-bithiophene (9)

A solution of **8** (1.50 g, 3.50 mmol), trimethylsilylacetylene (0.412 g, 4.20 mmol), $PdCl_2(PPh_3)_2$ (49.0 mg, 7.0×10^{-2} mmol), CuI (6.6 mg, 3.5×10^{-2} mmol), triphenylphosphane (92.0 mg, 0.35 mmol) and diethylamine (20 mL) was refluxed for 4 h. After cooling the solution to room temperature, the solvent was removed and diethyl ether (100 mL) was added. The organic layer was washed with water (3×80 mL) and dried over Na_2SO_4. After removing the solvent, the crude product was purified by flash chromatography (SiO_2, petroleum ether 40–60 °C/$CHCl_3$=2:1) to afford **9** in 80% yield as orange oil. MS (EI, 70 eV): m/z 446.2 (M^+), exact mass: 446.18 uma. ^{1}H NMR (400 MHz, $CDCl_3$): δ=7.72 (d, J=3.8 Hz, 1H), 7.20 (d, J=3.8 Hz, 1H), 7.15 (d, J=3.8 Hz, 1H), 7.13 (d, J=3.8 Hz, 1H), 4.30 (t, J=6.7 Hz, 2H), 1.76 (quint, J=6.7 Hz, 2H), 1.49–1.22 (m, 14H), 0.91 (t, J=7.0 Hz, 3H), 0.32 (s, 9H) ppm. ^{13}C{^{1}H} NMR (100 MHz, $CDCl_3$): δ=162.2, 144.1, 137.8, 134.0, 132.5, 128.0, 125.2, 123.7, 106.5, 91.7, 65.5, 31.9, 29.6, 29.5, 29.3, 28.7, 26.0, 22.7, 14.1, 0.2 ppm.

4.7. 5-Ethynyl-5′-carbodecaoxy-[2,2′]-bithiophene (10)

A mixture of **9** (1.16 g, 2.60 mmol), KF (155 mg, 13.00 mmol), CH_2Cl_2 (25 mL) and methanol (8 mL) was refluxed for 1 h. After cooling the solution to room temperature, the solvent was evaporated and diethyl ether (50 mL) was added. The resulting phase was washed with water (3×50 mL) and dried over Na_2SO_4. After removing the solvent, the crude product was purified by flash chromatography (SiO_2, petroleum ether 40–60 °C/CH_2Cl_2=2:1) to afford **10** in 95% yield as brown solid. ^{1}H NMR (400 MHz, $CDCl_3$): δ=7.70 (d, J=3.8 Hz, 1H), 7.21 (d, J=3.8 Hz, 1H), 7.16 (d, J=3.8 Hz, 1H), 7.15 (d, J=3.8 Hz, 1H), 4.30 (t, J=6.7 Hz, 2H), 3.46 (s, 1H), 1.76 (quint, J=6.7 Hz, 2H), 1.49–1.22 (m, 14H), 0.90 (t, J=7.0 Hz, 3H) ppm. ^{13}C{^{1}H} NMR (100 MHz, $CDCl_3$): δ=162.2, 144.0, 137.9, 134.0, 132.6, 128.1, 125.2, 123.9, 83.0, 76.5, 65.5, 31.9, 29.6, 29.5, 29.3, 28.7, 26.0, 22.7, 14.1 ppm.

4.8. 7,7‴-Bis(9,9-dihexylfluoren-2-yl-ethynyl)-[2′,2‴]-bis[spiro(cyclohexane-1,9′,1″,9‴-fluorene)] (SB1)

A mixture of **4** (0.215 g, 0.30 mmol), **5** (0.225 g, 0.63 mmol), $Pd(PPh_3)_4$ (69.3 mg, 0.06 mmol), CuI (11.4 mg, 0.06 mmol) and diethylamine (5 mL) was refluxed for 4 h. After cooling the solution to room temperature, diethyl ether (50 mL) was added and the resulting mixture was washed with water (3×30 mL) and dried over Na_2SO_4. After removing the solvent, the crude product was purified by flash chromatography (SiO_2, petroleum ether 40–60 °C/CH_2Cl_2=8:1) to afford **SB1** in 81% yield as pale-yellow solid. Anal. Calcd for $C_{90}H_{98}$: C, 91.63; H, 8.37. Found: C, 91.58; H, 8.40. ^{1}H NMR (400 MHz, $CDCl_3$): δ=7.92 (s, 4H), 7.83 (d, J=8.0 Hz, 2H), 7.77 (d, J=8.0 Hz, 2H), 7.73–7.66 (m, 6H), 7.62 (dd, J=8.0, 1.0 Hz, 2H), 7.59–7.55 (m, 4H), 7.38–7.30 (m, 6H), 2.10–1.95 (m, 16H), 1.94–1.79 (m, 12H), 1.19–0.99 (m, 24H), 0.78 (t, J=7.0 Hz, 12H), 0.72–0.54 (m, 8H) ppm. ^{13}C{^{1}H} NMR (100 MHz, $CDCl_3$): δ=154.3, 153.4, 151.0, 150.8, 141.4, 141.0, 140.5, 139.5, 138.2, 130.8, 130.6, 127.7, 127.5, 126.9, 126.5, 125.9, 123.4, 122.9, 121.6, 121.5, 120.4, 120.0, 119.9, 119.7, 90.7, 90.5, 55.2, 50.5, 40.5, 35.7, 31.6, 29.8, 25.6, 22.8, 22.6, 14.0 ppm. FTIR (KBr): ν=2922, 2852, 1453, 1256, 880, 816, 733 cm^{-1}.

4.9. 7,7‴-Bis-(*N*-hexylcarbazol-3-yl-ethynyl)-[2′,2‴]-bis[spiro(cyclohexane-1,9′,1″,9‴-fluorene)] (SB2)

A mixture of **4** (0.215 g, 0.30 mmol), **6** (0.173 g, 0.63 mmol), $Pd(PPh_3)_4$ (69.3 mg, 0.06 mmol), CuI (11.4 mg, 0.06 mmol) and diethylamine (5 mL) was refluxed for 4 h. After cooling the solution to room temperature, diethyl ether (50 mL) was added and the resulting mixture was washed with water (3×30 mL) and dried over Na_2SO_4. After removing the solvent, the crude product was purified by flash chromatography (SiO_2, petroleum ether 40–60 °C/CH_2Cl_2=3:1) to afford **SB2** in 81% yield as pale yellow solid. Anal. Calcd for $C_{76}H_{72}N_2$: C, 90.07; H, 7.16; N, 2.76. Found: C, 90.15; H, 7.11; N, 2.74. ^{1}H NMR (400 MHz, $CDCl_3$): δ=8.35 (d, J=1.3 Hz, 2H), 8.12 (d, J=7.7 Hz, 2H), 7.93–7.89 (m, 4H), 7.82 (d, J=8.0 Hz, 2H), 7.77 (d, J=7.7 Hz, 2H), 7.71–7.65 (m, 4H), 7.61 (dd, J=7.7, 1.3 Hz, 2H), 7.50 (td, J=8.0, 2.0 Hz, 2H), 7.44–7.37 (m, 4H), 7.27 (td, J=8.0, 2.0 Hz, 2H), 4.31 (t, J=7.0 Hz), 2.08–1.97 (m, 8H), 1.95–1.80 (m, 16H), 1.45–1.23 (m, 12H), 0.87 (t, J=7.0 Hz, 6H) ppm. ^{13}C{^{1}H} NMR (100 MHz, $CDCl_3$): δ=154.3, 153.4, 140.9, 140.8, 140.1, 139.1, 138.3, 130.6, 129.3, 127.7, 126.5, 126.1, 124.0, 123.4, 122.9, 122.5, 122.0, 120.6, 120.3, 119.8, 119.3, 108.9, 108.8, 90.9, 88.8, 50.4, 43.2, 35.7, 31.6, 29.0, 27.0, 25.6, 22.8, 22.6, 14.0 ppm. FTIR (KBr): ν=2927, 2855, 2197 (C≡C), 1595, 1475, 1342, 1248, 813, 736 cm^{-1}.

4.10. 7′-Iodo-7‴-(5-carbodecaoxy-[2,2′]-bithien-5′-yl-ethynyl)-[2′,2‴]-bis[spiro(cyclohexane-1,9′,1″,9‴-fluorene)] (15) and 7′,7‴-bis(5-carbodecaoxy-[2,2′]-bithien-5′-yl-ethynyl)-[2′,2‴]-bis[spiro(cyclohexane-1,9′,1″,9‴-fluorene)] (SB3)

A mixture of **4** (0.718 g, 1.00 mmol), **10** (0.375 g, 1.00 mmol), $Pd(PPh_3)_4$ (115.5 mg, 0.01 mmol), CuI (19.0 mg, 0.01 mmol) and diethylamine (15 mL) was refluxed overnight. After cooling the solution to room temperature, diethyl ether (50 mL) was added and the resulting mixture was washed with water (3×50 mL) and dried over Na_2SO_4. After removing the solvent, compound **11** was isolated by flash chromatography (SiO_2, petroleum ether 40–60 °C/CH_2Cl_2=1:1) in 27% yield as yellow solid and compound **SB3** was isolated by flash chromatography (SiO_2, petroleum ether 40–60 °C/CH_2Cl_2=1:2) in 17% yield as pale brown solid. Compound **11**: mp=110.3–111.9 °C. Anal. Calcd for $C_{57}H_{57}IO_2S_2$: C, 70.94; H, 5.95; S, 6.65. Found: C, 70.98; H, 5.91; S, 6.60. ^{1}H NMR (400 MHz, $CDCl_3$): δ=8.04 (d, J=1.3 Hz, 1H), 7.94–7.75 (m, 6H), 7.74–7.62 (m, 4H), 7.60–7.51 (m, 2H), 7.25 (d, J=3.8 Hz, 1H), 7.22 (d, J=3.8 Hz, 1H), 7.19 (d, J=3.8 Hz, 1H), 4.32 (t, J=6.7 Hz, 2H), 2.07–1.72 (m, 22H), 1.50–1.21 (m, 14H), 0.91 (t, J=7.0 Hz, 3H) ppm. ^{13}C{^{1}H} NMR (100 MHz, $CDCl_3$): δ=162.1, 155.6, 154.4, 153.4, 143.1, 141.1, 140.1, 138.9, 138.0, 137.8, 137.4, 136.0, 134.1, 133.7, 132.7, 130.6, 127.6, 126.5, 126.3, 125.1, 124.3, 124.0, 123.4, 121.6, 120.5, 120.2, 119.9, 96.2, 92.3, 82.3, 65.5, 50.6, 50.5, 35.6, 35.5, 31.9, 29.5, 29.4, 29.3, 28.7, 26.0, 25.4, 22.7, 22.6, 14.1 ppm. Compound **SB3**: Anal. Calcd for $C_{78}H_{82}O_4S_4$: C, 77.31; H, 6.82; S, 10.59. Found: C, 77.35; H, 6.83; S, 10.54. ^{1}H NMR (400 MHz, $CDCl_3$): δ=7.93–7.87 (m, 4H), 7.85 (d, J=7.9 Hz, 2H), 7.79 (d, J=7.9 Hz, 2H), 7.73 (d, J=3.8 Hz, 2H), 7.69 (dd, J=7.9, 1.6 Hz, 2H), 7.58 (dd, J=7.6, 1.3 Hz, 2H), 7.26 (d, J=3.8 Hz, 2H), 7.22 (d, J=3.8 Hz, 2H), 7.19 (d, J=3.8 Hz, 2H), 4.32 (t, J=6.4 Hz, 4H), 2.08, 1.98 (m, 8H), 1.96–1.73 (m, 16H), 1.50–1.23 (m, 28H), 0.91 (t, J=7.0 Hz, 6H) ppm. ^{13}C{^{1}H} NMR (100 MHz, $CDCl_3$): δ=162.1, 154.4, 153.4, 143.2, 141.1, 140.0, 138.0, 137.5, 132.3, 130.6, 127.6, 126.6, 125.1, 124.3, 124.1, 123.4, 120.6, 120.5, 119.9, 96.2, 82.4, 65.5, 50.5, 35.6, 31.9, 29.6, 29.3, 29.2, 28.7, 26.0, 25.5, 22.8, 22.7, 14.1 ppm. FTIR (KBr): ν=3067, 2923, 2855, 2188 (C≡C), 1703 (C=O), 1471, 1430, 1386, 1089, 824, 741 cm^{-1}.

4.11. 7′-(5-Carbodecaoxy-[2,2′]-bithien-5′-yl-ethynyl)-7‴-(*N*-hexylcarbazol-3-yl-ethynyl)-[2′,2‴]-bis[spiro(cyclohexane-1,9′,1″,9‴-fluorene)] (SB4)

A mixture of **11** (0.145 g, 0.15 mmol), **6** (47.7 mg, 0.17 mmol), $Pd(PPh_3)_4$ (20.0 mg, 1.7×10^{-2} mmol) and CuI (3.3 mg, 1.7×10^{-2} mmol) in diethylamine (5 mL) was refluxed overnight. After cooling the solution to room temperature, diethyl ether (50 mL) was added and the resulting mixture was washed with water (3×30 mL) and dried over Na_2SO_4. After removing the solvent, the crude product was purified by flash chromatography (SiO_2, petroleum ether 40–60 °C/CH_2Cl_2=3:1) to give **SB4** in 93% yield as yellow solid. Anal. Calcd for $C_{77}H_{77}NO_2S_2$: C, 83.12; H, 6.98; N, 1.26; S, 5.76. Found: C, 83.18; H, 6.94; N, 1.26; S, 5.77. ^{1}H NMR (400 MHz, $CDCl_3$): δ=8.38 (s, 1H), 8.15 (d, J=7.6 Hz, 1H), 7.98–7.91 (m, 3H), 7.89 (s, 1H), 7.84 (d, J=7.9 Hz, 2H), 7.78 (dd, J=7.9, 3.5 Hz, 2H), 7.75–7.67 (m, 3H), 7.64 (d, J=7.9 Hz, 1H), 7.56 (d, J=8.3 Hz, 1H), 7.53 (pt, J=7.9 Hz, 1H), 7.47–7.39 (m, 2H), 7.31 (d, J=7.6 Hz, 1H), 7.26 (d, J=3.5 Hz, 1H), 7.22 (d, J=3.5 Hz, 1H), 7.19 (d, J=3.5 Hz, 1H), 4.34–4.31 (m, 4H), 2.10–1.69 (m, 24H), 1.52–1.15 (m, 20H), 0.95–0.84 (m, 6H) ppm. ^{13}C{^{1}H} NMR (100 MHz, $CDCl_3$): δ=162.1, 154.4, 154.3, 153.4, 153.4, 143.2, 141.3, 140.8, 140.7, 140.1, 139.1, 138.4, 138.0, 134.1, 132.7, 132.3, 130.7, 130.6, 129.3, 127.7, 127.6, 126.6, 126.5, 126.1, 125.1, 124.2, 124.1, 124.0, 123.4, 122.9, 122.5, 122.1, 120.5, 120.4, 120.3, 119.9, 119.8, 119.3, 108.9, 108.8, 96.3, 91.0, 88.6, 82.4, 65.5, 50.5, 50.4, 43.2, 35.7, 35.6, 31.9, 31.6, 29.7, 29.6, 29.3, 29.2, 29.1, 29.0, 28.7, 27.2, 27.0, 26.0, 25.6, 25.0, 22.8, 22.7, 22.6, 14.2, 14.0 ppm. FTIR (KBr): ν=2925, 2856, 2002 (C≡C), 1695 (C=O), 1460, 1270, 1086, 877, 807, 737 cm^{-1}.

Acknowledgements

Dr. Paolo Pesce is gratefully acknowledged for laboratory assistance.

Supplementary data

This section contains the ^{1}H and ^{13}C{^{1}H} NMR spectra of **SB1**–**4**, and the ^{1}H–^{1}H COSY and ^{1}H–^{13}C HMQC of **1**. The EL spectra at different bias and the CV scans of **SB1**–**4** are also reported. Supplementary data associated with this article can be found in the online version, at doi:10.1016/j.tet.2008.06.098.

References and notes

1. Grimsdale, A. C.; Müllen, K. *Macromol. Rapid Commun.* **2007**, *28*, 1676–1702.
2. Leclerc, M. *J. Polym. Sci., Part A: Polym. Chem.* **2001**, *39*, 2867–2873.
3. (a) Becker, K.; Lupton, J. M.; Feldmann, J.; Nehls, B. S.; Galbrecht, F.; Gao, D.; Scherf, U. *Adv. Funct. Mater.* **2006**, *16*, 364–370; (b) Kulkarni, A. P.; Kong, X.; Jenekhe, S. A. *J. Phys. Chem. B* **2004**, *108*, 8689–8701; (c) Romaner, L.; Pogantsch, A.; Scandiucci de Freitas, P.; Scherf, U.; Gaal, M.; Zojer, E.; List, E. J. W. *Adv. Funct. Mater.* **2003**, *13*, 597–601.
4. (a) Jaramillo-Isaza, F.; Turner, M. L. *J. Mater. Chem.* **2006**, *16*, 83–89; (b) Sims, M.; Bradley, D. D. C.; Ariu, M.; Koeberg, M.; Asimakis, A.; Grell, M.; Lidzey, D. G. *Adv. Funct. Mater.* **2004**, *14*, 765–781.
5. (a) Chi, C.; Im, C.; Enkelmann, V.; Ziegler, A.; Lieser, G.; Wegner, G. *Chem.—Eur. J.* **2005**, *11*, 6833–6845; (b) Zojer, E.; Pogantsch, A.; Hennebicq, E.; Beljonne, D.; Brédas, J.-L.; Scandiucci de Freitas, P.; Scherf, U.; List, E. J. W. *J. Chem. Phys.* **2002**, *117*, 6794–6802; (c) Craig, M. R.; de Kok, M. M.; Hofstraat, J. W.; Schenning, A. P. H. J.; Meijer, E. W. *J. Mater. Chem.* **2003**, *13*, 2861–2862; (d) Cho, S. Y.; Grimsdale, A. C.; Jones, D. J.; Watkins, S. E.; Holmes, A. B. *J. Am. Chem. Soc.* **2007**, *129*, 11910–11911.
6. Mullen, K.; Wegner, G. *Electronic Materials: The Oligomer Approach*; Wiley-VCH: Weinheim, 1998.
7. (a) Culligan, S. W.; Geng, Y.; Chen, S. H.; Klubek, K.; Vaeth, K. M.; Tang, C. W. *Adv. Mater.* **2003**, *15*, 1176–1180; (b) Geng, Y.; Culligan, S. W.; Trajkovska, A.; Wallace, J. U.; Chen, S. H. *Chem. Mater.* **2003**, *15*, 542–549; (c) Katsis, D.; Geng, Y. H.; Ou, J. J.; Culligan, S. W.; Trajkovska, A.; Chen, S. H.; Rothberg, L. J. *Chem. Mater.* **2002**, *14*, 1332–1339; (d) Geng, Y.; Katsis, D.; Culligan, S. W.; Ou, J. J.; Chen, S. H.; Rothberg, L. J. *Chem. Mater.* **2002**, *14*, 463–470; (e) Wong, K.-T.; Chien, Y.-Y.; Chen, R.-T.; Wang, C.-F.; Lin, Y.-T.; Chiang, H.-H.; Hsieh, P.-Y.; Wu, C.-C.; Chou, C. H.; Su, Y. O.; Lee, G.-H.; Peng, S.-M. *J. Am. Chem. Soc.* **2002**, *124*, 11576–11577.
8. (a) Li, Z. H.; Wong, M. S.; Fukutani, H.; Tao, Y. *Org. Lett.* **2006**, *8*, 4271–4274; (b) Li, Z. H.; Wong, M. S.; Tao, Y.; Lu, J. *Chem.—Eur. J.* **2005**, *11*, 3285–3293; (c) Zhang, Q.; Chen, J. S.; Cheng, Y. X.; Geng, Y. H.; Wang, L. X.; Ma, D. G.; Jing, X. B.; Wang, F. S. *Synth. Met.* **2005**, *152*, 229–232.
9. Saragi, T. P. I.; Spehr, T.; Siebert, A.; Fuhrmann-Lieker, T.; Salbeck, J. *Chem. Rev.* **2007**, *107*, 1011–1065.
10. (a) Grisorio, R.; Mastrorilli, P.; Nobile, C. F.; Suranna, G. P. *Adv. Funct. Mater.* **2007**, *17*, 538–548; (b) Grisorio, R.; Mastrorilli, P.; Nobile, C. F.; Romanazzi, G.; Suranna, G. P.; Acierno, D.; Amendola, E. *Macromol. Chem. Phys.* **2005**, *206*, 448–455.
11. (a) Grisorio, R.; Dell'Aquila, A.; Romanazzi, G.; Suranna, G. P.; Mastrorilli, P.; Cosma, P.; Acierno, D.; Amendola, E.; Ciccarella, G.; Nobile, C. F. *Tetrahedron* **2006**, *62*, 627–634; (b) Chao, T.-C.; Lin, Y.-T.; Yang, C.-Y.; Hung, T. S.; Chou, H.-C.; Wu, C.-C.; Wong, K.-T. *Adv. Mater.* **2005**, *17*, 992–996.
12. (a) Lee, S. H.; Nakamura, T.; Tsutsui, T. *Org. Lett.* **2001**, *3*, 2005–2008; (b) Zhao, Z.; Xu, X.; Wang, F.; Yu, G.; Lu, P.; Liu, Y.; Zhu, D. *Synth. Met.* **2006**, *156*, 209–212; (c) Dias, F. B.; Pollock, S.; Hedley, G.; Palsson, L.-O.; Monkman, A.; Perepichka, I. I.; Perepichka, I. F.; Tavasli, M.; Bryce, M. R. *J. Phys. Chem. B* **2006**, *110*, 19329–19339; (d) Rathnayake, H. P.; Cirpan, A.; Delen, Z.; Lahti, P. M.; Karasz, F. E. *Adv. Funct. Mater.* **2007**, *17*, 115–122; (e) Mikroyannidis, J. A.; Fenenko, L.; Adachi, C. *J. Phys. Chem. B* **2006**, *110*, 20317–20326; (f) Morales, A. R.; Belfield, K. D.; Hales, J. M.; Van Stryland, E. W.; Hagan, D. J. *Chem. Mater.* **2006**, *18*, 4972–4980.
13. Grisorio, R.; Mastrorilli, P.; Nobile, C. F.; Romanazzi, G.; Suranna, G. P.; Meijer, E. W. *Tetrahedron Lett.* **2004**, *45*, 5367–5370.
14. Grisorio, R.; Piliego, C.; Fini, P.; Cosma, P.; Mastrorilli, P.; Gigli, G.; Suranna, G. P.; Nobile, C. F. *J. Phys. Chem. C* **2008**, *112*, 7005–7014.
15. Melucci, M.; Frère, P.; Allain, M.; Levillain, E.; Barbarella, G.; Roncali, J. *Tetrahedron* **2007**, *63*, 9774–9783.
16. Demas, J. N.; Crosby, G. A. *J. Phys. Chem.* **1971**, *75*, 991–1024.
17. de Leeuw, D. M.; Simenon, M. M. J.; Brown, A. R.; Einerhand, R. E. F. *Synth. Met.* **1997**, *87*, 53–59.
18. Kilbinger, A. F. M.; Schenning, A. P. H. J.; Goldoni, F.; Feast, W. J.; Meijer, E. W. *J. Am. Chem. Soc.* **2000**, *122*, 1820–1821.